International Journal of Nanomedicine

Dovepress
open access to scientific and medical research

Open Access Full Text Article

ORIGINAL RESEARCH

Noninvasive Molecular Imaging of the Enhanced Permeability and Retention Effect by ^{64}Cu-Liposomes: In vivo Correlations with ^{68}Ga-RGD, Fluid Pressure, Diffusivity and ^{18}F-FDG

This article was published in the following Dove Press journal:
International Journal of Nanomedicine

Betina Børresen[1]
Anders Elias Hansen[2,3]
Frederikke Petrine Fliedner[2]
Jonas Rosager Henriksen[3]
Dennis Ringkjøbing Elema[3,4]
Malene Brandt-Larsen[5]
Lotte Kellemann Kristensen[2–6]
Annemarie Thuri Kristensen[1–6]
Thomas Lars Andresen[3]
Andreas Kjær[2,5]

[1]Department of Veterinary Clinical Sciences, Faculty of Health and Medical Sciences, University of Copenhagen, Frederiksberg C 1870, Denmark; [2]Cluster for Molecular Imaging, Department of Biomedical Sciences, Faculty of Health and Medical Sciences, University of Copenhagen, Copenhagen N 2200, Denmark; [3]DTU Health Technology, Center for Nanomedicine and Theranostics, Technical University of Denmark, Lyngby, Kgs 2800, Denmark; [4]DTU Health Technology, The Hevesy Laboratory, Center for Nuclear Technologies, Technical University of Denmark, Roskilde, 4000, Denmark; [5]Department of Clinical Physiology, Nuclear Medicine and PET, Copenhagen University Hospital, Copenhagen Ø 2100, Denmark; [6]Minerva Imaging, Copenhagen N 2200, Denmark

Correspondence: Andreas Kjær
Cluster for Molecular Imaging, Department of Biomedical Sciences, Faculty of Health and Medical Sciences, University of Copenhagen, Blegdamsvej 3, Copenhagen N 2200, Denmark
Tel +45 35 32 75 04
Fax +45 35 32 75 46
Email akjaer@sund.ku.dk

Background: The accumulation of liposome encapsulated chemotherapy in solid cancers is dependent on the presence of the enhanced permeability and retention (EPR) effect. Positron emission tomography (PET) imaging with a liposome encapsulated radioisotope, such as liposome encapsulated Cu-64 (^{64}Cu-liposome) may help to identify tumors with high liposome accumulation, and thereby stratify patients based on expected benefit from liposomal chemotherapy. However, intravenous administration of liposomes without a cytotoxic content is complicated by the accelerated blood clearance (ABC) phenomenon for succeeding therapeutic liposome dosing. Alternative markers for assessing the tumor's EPR level are therefore warranted.

Materials and Methods: To increase our understanding of EPR variations and to ultimately identify an alternative marker for the EPR effect, we investigated the correlation between ^{64}Cu-liposome PET/CT (EPR effect) and ^{68}Ga-RGD PET/CT (neoangiogenesis), ^{18}F-FDG PET/CT (glycolysis), diffusion-weighted MRI (diffusivity) and interstitial fluid pressure in two experimental cancer models (CT26 and COLO 205).

Results: ^{64}Cu-liposome and ^{68}Ga-RGD SUV_{max} displayed a significant moderate correlation, however, none of the other parameters evaluated displayed significant correlations. These results indicate that differences in neoangiogenesis may explain some EPR variability, however, as correlations were only moderate and not observed for SUV_{mean}, ^{68}Ga-RGD is probably insufficient to serve as a stand-alone surrogate marker for quantifying the EPR effect and stratifying patients.

Keywords: EPR effect, liposome, positron emission tomography, neoangiogenesis

Introduction

The enhanced permeability and retention (EPR) effect was defined by Matsumura and Maeda as an intratumoral phenomenon resulting from the increased leakiness of newly forming tumor vessels as well as decreased lymphatic drainage.[1] Therapy based on the EPR effect has not been the expected success,[2] possibly due to individual patient EPR variations, and patient stratification might be central to fully exploit the therapeutic potential of liposomal drugs. Macromolecular accumulation, based on the proposed presence of the EPR-effect, has been shown in human

tumors by gamma camera imaging, single photon emission computed tomography (SPECT) and positron emission tomography (PET).[3–8] We have performed extensive studies of the EPR effect using a radiolabeled ^{64}Cu-liposome formulation.[9] Based on PET/CT imaging of spontaneous malignant tumors in canine cancer patients, we have demonstrated that the EPR-effect is not ubiquitous, even for tumors with a similar histopathology.[10] Molecular imaging techniques, such as ^{64}Cu-liposome PET/CT, could potentially serve as the basis for selecting patients with a high EPR effect for liposome based chemotherapy (the theranostic principle), as has already been shown clinically.[7] This has a large potential for improving the response rates to liposomal chemotherapy.[11] However, for liposomes to accumulate via the EPR effect in solid tumors, a long circulating half-life is mandatory. This is generally achieved by decorating liposomes with varying levels and lengths of polyethylene glycol (PEG), a method known as PEGylation.[12] Unfortunately, PEG decoration has the ability to induce the formation of anti-PEG IgM antibodies.[13] Anti-PEG antibody formation is highly problematic for subsequent administrations of PEGylated liposomes, as it leads to a rapid liposome clearance, and thereby eliminates the possibility to achieve EPR dependent tumor accumulation. This problem has been termed "the accelerated blood clearance (ABC) phenomenon" and is well described in experimental animals.[14] Most PEGylated liposomes containing chemotherapeutics do not seem to induce anti-PEG antibodies, probably because the B-cells responsible for producing anti-PEG antibodies do not survive exposure to liposomal chemotherapy.[15,16] Importantly, however, a recent publication by our group demonstrated that EPR imaging with ^{64}Cu-liposome PET/CT will induce the ABC phenomenon in a canine cancer patients and in rats.[17] This means that performing pretreatment imaging of the EPR effect with ^{64}Cu-liposome for detecting those patients suitable for liposomal chemotherapy may actually "vaccinate" the patients against their treatment with potential decreased treatment response and increased toxicity as a consequence. Accordingly, alternative or surrogate markers, not based on PEGylated nanoparticles, for identifying tumors positive for the EPR effect is highly warranted.

The theoretical foundation for the EPR effect is based on the permeable characteristics of newly formed tumor vessels, hence tumor neoangiogenesis could potentially be an indirect marker for the EPR effect. Additionally, variations in liposome accumulation and the EPR effect might also be related to local microenvironmental factors, such as interstitial fluid pressure or diffusivity, that will affect the extravasation and transport of the nanoparticle.[18,19] As the EPR effect is theoretically related to tumor growth, fast-growing tumors with a high glycolytic activity could also have a high EPR effect and accordingly, tumor glycolysis may correlate with the level of EPR effect.

Tumor angiogenesis can be determined in vivo by non-invasive PET imaging. The $\alpha_V\beta_3$ integrin is a heterodimeric cell surface receptor that is overexpressed on activated endothelial cells during the process of angiogenesis, as well as on some tumor cells.[20,21] Arg-Gly-Asp (RGD) angiogenesis radiotracers targeting the $\alpha_V\beta_3$ integrin have been thoroughly investigated[22–24] and recently, a novel dimeric ^{68}Ga-RGD radiotracer was shown to have specificity towards the $\alpha_V\beta_3$ integrin in experimental cancer models.[25] Similarly, in vivo methods for the determining the interstitial fluid pressure, glycolytic activity and diffusivity are established.[26–28]

In the present study, we aimed to investigate the correlation between the degree of EPR-effect (^{64}Cu-liposome) and tumor neoangiogenesis (^{68}Ga-RGD), fluid pressure, glycolytic activity (^{18}F-FDG) and diffusivity (diffusion-weighted MRI) to identify potential biomarkers suitable for identification of the EPR effect. We observed that neoangiogenesis and the EPR effect are in fact correlated, however, none of the other tumor microenvironmental factors investigated in this study could explain the EPR variations and consequently, no other factors were deemed suitable as surrogate markers for the EPR effect.

Materials and Methods

Study Design

The first part of the study (part one) was designed to investigate the correlation between neoangiogenesis and the EPR-effect. This included ^{68}Ga-NODAGA-E[c(RGDyK)]$_2$ (^{68}Ga-RGD) microPET/CT, liposome encapsulated ^{64}Cu (^{64}Cu-liposome) microPET/CT and dual-tracer (^{68}Ga/^{64}Cu) gamma counting.

The second part of the study (part two) focused on other possible factors influencing the EPR-effect. This included ^{64}Cu-liposome microPET/CT, 2-deoxy-2-(^{18}F) fluoro-D-glucose (^{18}F-FDG) microPET/CT, diffusion-weighted MRI (dw-MRI) and interstitial fluid pressure (IFP) measurements.

The various PET/CT scans were performed on succeeding days, but with sufficient time interval between them to allow for adequate decay of the previous

radioisotope. For study part one, ^{68}Ga-RGD PET/CT was performed on day 1, ^{64}Cu-liposome PET/CT performed on day 2 and 3 and dual-tracer gamma counting performed on day 3. For study part two, ^{18}F-FDG PET/CT was performed on day 1, ^{64}Cu-liposome PET/CT performed on day 2 and 3 and dw-MRI and IFP measurements performed on day 3.

The experiments and all procedures were approved by The National Animal Experiments Inspectorate.

Cell Lines and Experimental Model

Two colorectal carcinoma models (COLO 205 and CT26) were investigated in a xenogeneic and syngeneic tumor microenvironment. Neither of the two cell types express the $\alpha_v\beta_3$ integrin on the surface.[29,30] Both cell lines were purchased from ATCC (Manassas, Virginia, US). Tumor models were established in acclimatized six weeks old female mice; NMRI nude (Taconic, Lille Skensved, Denmark) for COLO 205 tumors and BALB/c (Charles River, Scanbur A/S, Karlslunde, Denmark) for CT26 tumors. The mice were inoculated bilaterally in the subcutaneous flank region with 7×10^6 COLO 205 cells or 3×10^5 CT26 cells. The tumors were allowed to grow for two weeks prior to experimental procedures.

In the part one study, 12 BALB/c and 8 NMRI mice were included. In the part two study, 8 BALB/c mice and 8 NMRI mice were included. All study procedures were approved by the Danish Experimental Animal Inspectorate and institutional animal experiment committee. The guidelines followed for the welfare of the laboratory animals were those established by the Danish Experimental Animal Inspectorate.

Radiotracers

The ^{18}F-FDG radiotracer was obtained from the PET & Cyclotron Unit at Copenhagen University Hospital (Rigshospitalet, Copenhagen, Denmark) as the standard formulation for use in clinical diagnostics.

The ^{68}Ga-RGD was produced at the PET & Cyclotron Unit at Copenhagen University Hospital (Rigshospitalet, Copenhagen, Denmark). The NODAGA-E[c(RGDyK)]$_2$ acetate was obtained from ABX GmbH. Gallium-68 ($t_{1/2}$ = 68 min; $E_{max,\ \beta+}$ = 1.90 MeV (89%)) labelling of NODAGA-E[c(RGDyK)]$_2$ acetate was performed using a Modular-Lab eazy module (Eckert & Ziegler). The ^{68}Ge/^{68}Ga generator (IGG100, Eckert & Ziegler) was eluted with 6 mL 0.1M HCl. The eluate was concentrated on a Bond Elut SCX cartridge and eluted with 600 µL 5M NaCl/5.5M HCl (41:1). NODAGA-E[c(RGDyK)]$_2$ (30 nmol) was labelled in 1000 µL 0.7M NaOAc buffer pH 4.5 and 400 µL 50% EtOH at 60°C for 400 s. The resulting ^{68}Ga-NODAGA-E[c(RGDyK)]$_2$ was formulated with saline. The radiochemical purity was more than 93% pure on HPLC, and the amount of unlabeled ^{68}Ga in the product was less than 1%, as demonstrated by radio-thin layer chromatography. All reagents and cassettes were purchased from Eckert & Ziegler. For analysis, a high-performance liquid chromatograph (Ultimate 3000; Dionex) was used with a 2.6 µm, 100 Å, 50 × 4.6 mm C18 column (Kinetex). The mobile phases were: eluent A: 10% MeCN in H_2O with 0.1% trifluoroacetic acid; eluent B: 10% H_2O in MeCN with 0.1% trifluoroacetic acid.

The ^{64}Cu-liposome radiotracer was produced at Hevesy Laboratory, DTU Nutech (Technical University of Denmark, Roskilde, Denmark) in collaboration with DTU Health Tech (Technical University of Denmark, Lyngby, Denmark), as described previously.[10,31] The average size of the liposomes was 102 nm with a polydispersity index of 0.044 when measured by dynamic light scattering. The liposomes were loaded with an efficiency of >98.5% (evaluated by radio-HPLC and radio-TLC) and had an activity- and lipid-concentration of 62.5 MBq/mL and 13.2 mM, respectively, at the time of injection.

MicroPET/CT

The mice were anesthetized for all procedures using a sevoflurane gas-mixture (Sevorane®, Abbott Laboratories) in 35%O_2/65%N_2.

Combined PET/CT imaging was performed using a dedicated small animal microPET/CT scanner (Inveon, Siemens, Erlangen, Germany). For all PET scans, radiotracer activity was measured in the syringe and associated equipment before and after injection, and all parameters were recorded. All PET scans were performed directly following a whole-body CT scan with attenuation correction for reconstruction.

^{64}Cu-liposome microPET imaging was performed in both study parts on two consecutive days at 1 hour post-injection (pi.) and 24 hours pi. At one hour prior to the early PET scan, ^{64}Cu-liposome was injected using a tail vein. The mice received approximately 10 Mbq (range 8.6–12.4) ^{64}Cu per mouse. The PET scans were conducted as whole body list mode for 5 minutes (1 hour pi.) and 15 minutes (24 hour pi.). The 24 hour pi. ^{64}Cu-liposome tumor uptake was assumed to primarily depict the EPR effect, as sufficient time had passed for the liposomes to

clear the vasculature and distribute into the tumor interstitium.[10]

One hour prior to FDG PET/CT imaging, approximately 10 Mbq (range 7.0–10.4) of ^{18}F-FDG was injected per mouse. The scans were conducted as whole body list mode for 5 minutes.

^{68}Ga-RGD microPET/CT was performed one hour after the injection of 1.3–3.2 MBq ^{68}Ga-RGD per animal. Each animal received approximately 0.2 nmol peptide in total. The scans were conducted as whole body list mode for 7.5 minutes.

All PET scans were reconstructed using a maximum a posteriori reconstruction algorithm with a voxel size of 0.400 mm x 0.400 mm x 0.796 mm and a resolution (FWHM) of 1.5 mm. The PET/CT images were rigidly co-registered in the Inveon Research Workspace software (Siemens Healthcare, Erlangen, Germany). Tumors were manually delineated based on combined PET/CT images, and PET uptake in the tumor region of interest (ROI) was quantified using standardized uptake values (SUV) and expressed as mean and maximum ± SD.

Diffusion-Weighted Magnetic Resonance Imaging

MRI was acquired on the Bruker 7T BioSpec Pharmascan preclinical system (Bruker, Ettlingen, Germany) using a 20 mm planar RF surface coil. Mice were anesthetized for the MRI session using the same procedure as for PET/CT, and body temperature was maintained stable during scans. A diffusion-weighted EPI scan sequence with the following parameters was used; Repetition time (TR)/Echo time (TE); 550/24 ms, image size; 96x96, Field of view (FOV); 30x30, averages; 6, segments; 6, slice no.; 5, slice thickness; 0.7 mm, b-values; 0, 100, 200, 600, 1000, 1500, 2000, and scan time 2 minutes 18 seconds.

Image analysis and apparent diffusion coefficient (ADC)-calculations were made using the ParaVision 6.0.1. software (Bruker, Ettlingen, Germany). ROIs encapsulating the whole tumor area were defined manually in one chosen sagittal scan slice placed in the center of the tumor. Tissue ADC-values within the specified ROI were calculated from bi-exponential signal intensity plot fitting by the ParaVision software.

Tumor Interstitial Fluid Pressure

IFP measurement was the last procedure prior to sacrificing the mice. The mice were anesthetized using the previously described protocol. The Millar Catheter SPR 320 system (Millar Inc, Houston, USA) was used by carefully pre-inserting a 21 gauge needle into the tumor center and then introducing the Micro-Tip Transducer via the needle tract. The transducer was left in the tumor center until a stable pressure reading was observed. The pressure catheter was connected to a computer using a Millar TC-510 control unit (Millar Inc, Houston, USA). Pressure data (mmHg) acquisition was performed using the LabView software (National Instruments, Houston, USA).

Gamma Counted Uptake of ^{68}Ga-RGD and ^{64}Cu-Liposome

To validate results from the PET/CT studies, as well as to evaluate correlations between ^{64}Cu-liposome and ^{68}Ga-RGD at the micro-regional level, tracer uptake was also measured by gamma counting. In study part one, after the 24 hour ^{64}Cu-liposome PET/CT scan, the mice were re-injected with ^{68}Ga-RGD (0.65–0.8 MBq per mouse) and euthanized one hour later. All tumors were cut into multiple small pieces of less than 40 mg and weighed in gamma counting tubes. These were then activity measured twice using a Wizard 2.3" automatic gamma counter (PerkinElmer, Waltham, MA, USA) approximately 21 hours apart to exploit the different half-lives of ^{68}Ga and ^{64}Cu. Counting time was 60 seconds at 0 hour and 120 seconds at 21 hour. The counting efficacy was 9.43% for ^{64}Cu and 47.3% for ^{68}Ga. Activity of ^{68}Ga was assumed to be zero at the 21 hour time point. The activity was given as percent of injected dose per gram tissue (ID%/g).

Statistical Analysis

All statistical analyses were performed in GraphPad Prism 6.0. Correlations were tested using a two-sided nonparametric Spearman's analysis. For all statistical analyses, a p-value of 0.05 was considered significant.

Results

All tumors displayed uptake of both ^{68}Ga-RGD and ^{18}F-FDG, and had a clear increase in tumor ^{64}Cu-liposome accumulation from the 1 hour to the 24 hour imaging session. IFP measurements, dw-MRI imaging and subsequent analysis were successfully performed in study part two. Results are given in Figure 1. A representative example showing the ^{68}Ga-RGD PET/CT, the 1 hour ^{64}Cu-liposome PET/CT and the 24 hour ^{64}Cu-liposome PET/CT from the same mouse in study part one as well as

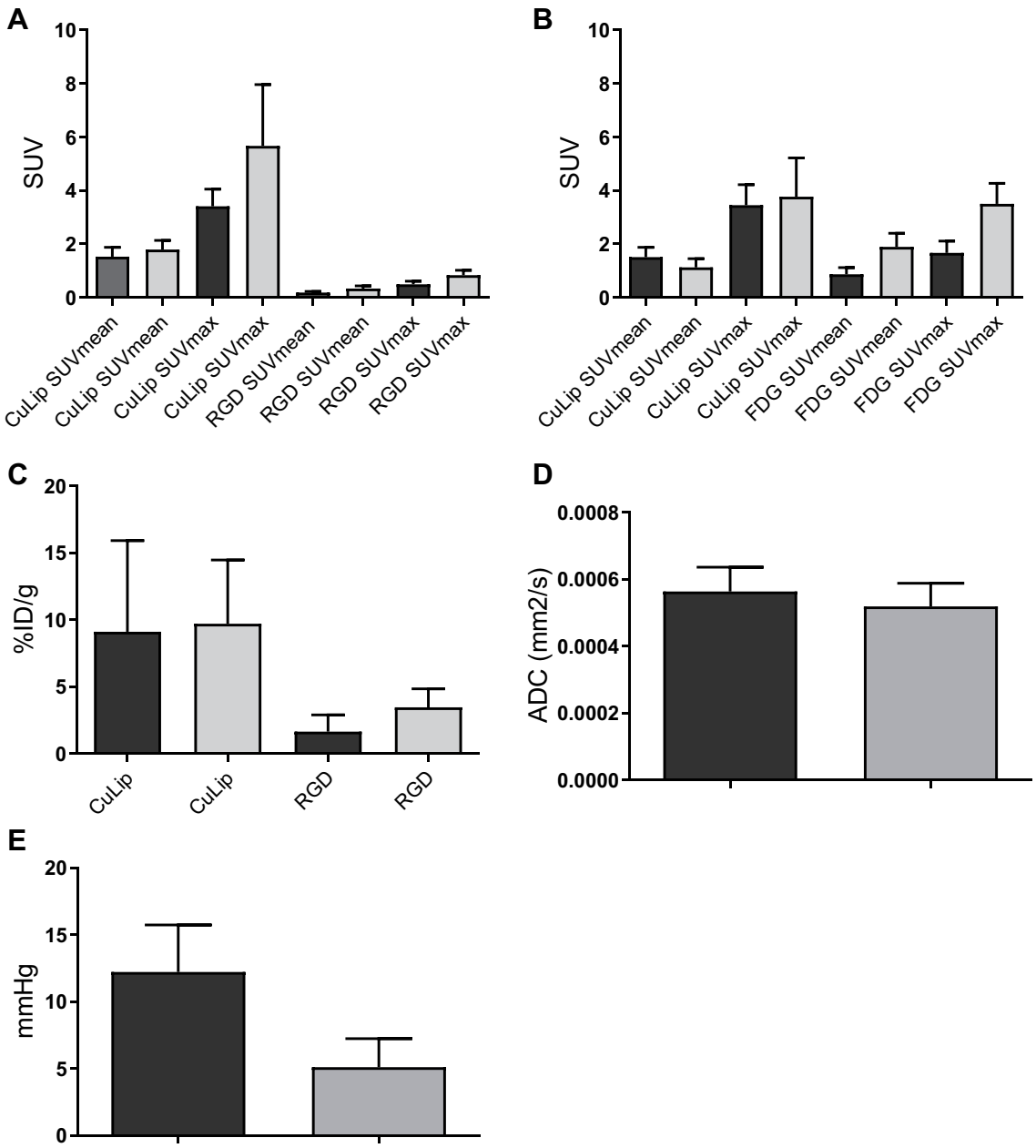

Figure 1 Tumor tracer uptake, interstitial fluid pressure and diffusivity at study part one and two for COLO 205 and CT26 tumors showing mean and SD values. PET uptake data (SUV_{mean} and SUV_{max}) in study part one for 24h CuLip (^{64}Cu-liposome) and RGD (**A**), PET uptake data (SUV_{mean} and SUV_{max}) in study part two for 24h CuLip and FDG (**B**), gamma counted data (%ID/g) for 24h CuLip and RGD (**C**), dwMRI data (ADC mm^2/s) (**D**) and IFP data (mmHg) (**E**). COLO 205 is dark grey and CT26 light grey.

representative dw-MRI images are illustrated in Figure 2. Similarly, a representative image from a mouse in study part two showing ^{18}F-FDG PET/CT, the 1 hour ^{64}Cu-liposome and the 24 hour ^{64}Cu-liposome PET/CT as well as representative dw-MRI images is illustrated in Figure 3.

Spearman correlation parameters between the 24 hour pi. ^{64}Cu-liposome tumor activity and ^{68}Ga-RGD, ^{18}F-FDG, dw-MRI and IFP levels are listed in Table 1. The 24 hour PET SUV_{max} uptake of ^{64}Cu-liposome activity displayed a moderate positive correlation to SUV_{max} uptake of ^{68}Ga-RGD for both CT26 and COLO 205 tumors. However, no significant correlation was observed between the ^{64}Cu-liposome and ^{68}Ga-RGD SUV_{mean} uptake for neither CT26 nor COLO 205 tumors. Importantly, when sectioning tumors into multiple smaller sections and gamma counting these, a significant moderate correlation between gamma counted activity of ^{68}Ga-RGD and ^{64}Cu-liposome %ID/

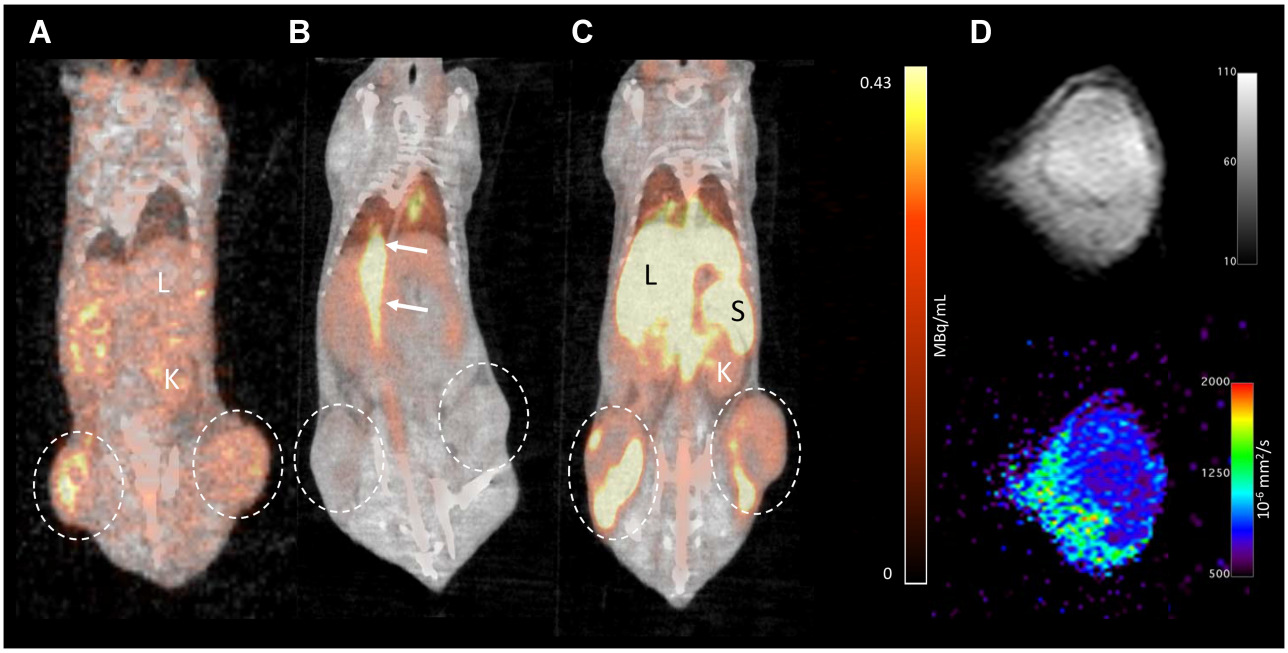

Figure 2 Representative PET/CT examples of the same BALB/c mouse with CT26 tumor xenografts, showing the ^{68}Ga-RGD PET/CT (**A**), 1 hour ^{64}Cu-liposome PET/CT (**B**) and 24 hour ^{64}Cu-liposome PET/CT (**C**). The circles depict tumor uptake, the arrows depict vascular uptake and the L, S and K depict hepatic, splenic and renal uptake, respectively. Right side of figure (**D**) shows a representative DWI image from shortest b-value (b=0) (top) and an ADC-map calculated from bi-exponential signal intensity plot fitting (bottom).

g was identified for both CT26 and COLO 205 tumors (Figure 4). Despite the expected influence of IFP, diffusivity and metabolic activity, no significant correlations were found between ^{64}Cu-liposome accumulation and intratumoral IFP, dw-MRI or ^{18}F-FDG for either of the tumor types.

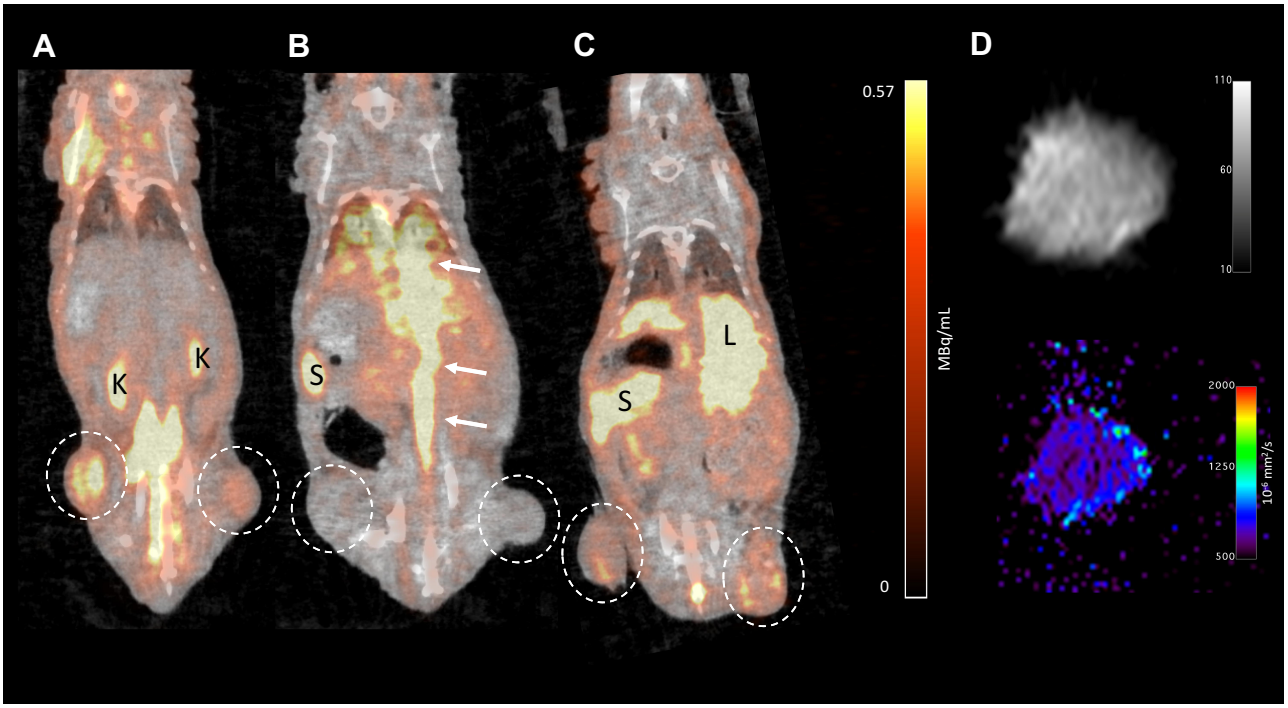

Figure 3 Representative PET/CT examples of the same NMRI mouse with COLO 205 tumor xenografts, showing the ^{18}F-FDG PET/CT (**A**), 1 hour ^{64}Cu-liposome PET/CT (**B**) and 24 hour ^{64}Cu-liposome PET/CT (**C**). The circles depict tumor uptake, the arrows depict vascular uptake and the L, S and K depict hepatic, splenic and renal uptake, respectively. Right side of figure (**D**) shows a representative DWI image from shortest b-value (b=0) (top) and an ADC-map calculated from bi-exponential signal intensity plot fitting (bottom).

Table 1 Spearman Correlations Parameters Comparing Tumor 24 Hour Uptake of ^{64}Cu-Liposome to ^{68}Ga-RGD Uptake, ^{18}F-FDG, Interstitial Fluid Pressure and Diffusion-Weighted MRI

		COLO 205		CT26	
		r	p	r	p
Part one	SUV_{max} 24h CuLip vs RGD	0.57	**0.03**	0.45	**0.01**
	SUV_{mean} 24h CuLip vs RGD	0.36	0.19	−0.10	0.59
	ID%/g GC 24h CuLip vs GC RGD	0.40	**<0.002**	0.44	**<0.0001**
Part two	SUV_{max} 24h CuLip vs FDG	0.07	0.80	0.34	0.29
	SUV_{mean} 24h CuLip vs FDG	−0.30	0.30	−0.23	0.44
	SUV_{max} 24h CuLip vs IFP	−0.18	0.51	−0.23	0.51
	SUV_{mean} 24h CuLip vs IFP	−0.22	0.42	−0.41	0.21
	SUV_{max} 24h CuLip vs DWI	0.20	0.50	−0.03	0.95
	SUV_{mean} 24h CuLip vs DWI	0.37	0.19	−0.06	0.87

Notes: Significant results in bold.
Abbreviations: CuLip: ^{64}Cu-liposome. GC: gamma counted data. IFP: interstitial fluid pressure. DWI: diffusion weighted MRI.

Discussion

Imaging of the EPR effect may provide information for selecting patients suitable for liposomal chemotherapy, however, PEGylated liposomal radiotracers may induce the ABC phenomenon.[17] Tumor microenvironmental factors affecting the local EPR effect could potentially become novel surrogate markers for identifying the EPR effect and thereby eliminate the ABC problems associated with the direct use of labeled PEGylated liposomes for imaging.

Tumor liposome accumulation has previously been shown to be related to various indirect markers of neoangiogenesis,[32–37] and the abnormal architecture including dilatations and wide fenestrations of neoangiogenic tumor vessels are an important part of the theoretical basis for the EPR-effect.[38] Accordingly, ^{68}Ga-RGD could potentially estimate the level of EPR-effect in solid tumors. In line with this, we observed a positive correlation between maximum ^{68}Ga-RGD and maximum 24 hour pi. ^{64}Cu-liposome (EPR) uptake, but no correlation for tumor mean radiotracer uptake (Figure 4). To substantiate these results, dual-tracer gamma counting of very small tumor pieces was performed, and it was observed that ^{68}Ga-RGD and ^{64}Cu-liposome accumulation also correlate positively at the micro regional level (Figure 4). This observation underlines the potential of these results and verifies that tumor liposome accumulation and tumor neoangiogenesis are associated to some degree.

The correlations between maximum PET uptake and gamma counted activity of ^{68}Ga-RGD and ^{64}Cu-liposome were only moderate (r=0.57 for COLO 205 and r=0.45 for CT26, Table 1), suggesting that variations in neoangiogenesis alone cannot explain variations in liposome accumulation, and hence that ^{68}Ga-RGD uptake is probably not an optimal surrogate marker for the EPR effect. Accordingly, we investigated other factors that may influence the EPR effect.

High vascular permeability and low lymphatic drainage are permitting for the extravascular leakage and decreased clearance of nanoparticles that form the basis for the EPR effect. However, fluid and macromolecules accumulate concurrently, and an increase in IFP is expected for the same reasons.[2] The transvascular convective transport of liposomes is dependent on the difference between vascular hydrostatic pressure and tumoral interstitial fluid pressure, and in the case of a very high IFP, the driving force for extravasation of liposomes may be decreased or even lacking.[19] Based on this, an inverse correlation between IFP and liposome accumulation was expected in this study, and although we did observe a negative correlation in both tumor types, this was weak and statistically insignificant (Table 1). Also, COLO 205 tumors had a markedly higher IFP than CT26 tumors (Figure 1), but this did not correspond to a consistently lower ^{64}Cu-liposome uptake. This result was surprising, as an elevated tumor interstitial fluid pressure should reduce the convective transport of nanoparticles as well as other large molecules.[39] A plausible explanation for the lack of a clear negative correlation between IFP and liposome-accumulation could simply be that, due to the inherent relationship between high vascular permeability (and thereby the EPR effect) and high IFP, tumors with a high IFP are also those tumors with a high EPR effect. This means that the expected low liposome accumulation associated with a high IFP would be attenuated, causing the weak and insignificant negative correlation observed in this study. Also, we sampled IFP only once from a central area in each tumor, which may have been insufficient. However, Gulliksrud et al showed that repeated central measurements have limited variation, and that a single measurement should be representative for tumoral IFP.[40] Despite this, it has also been shown that

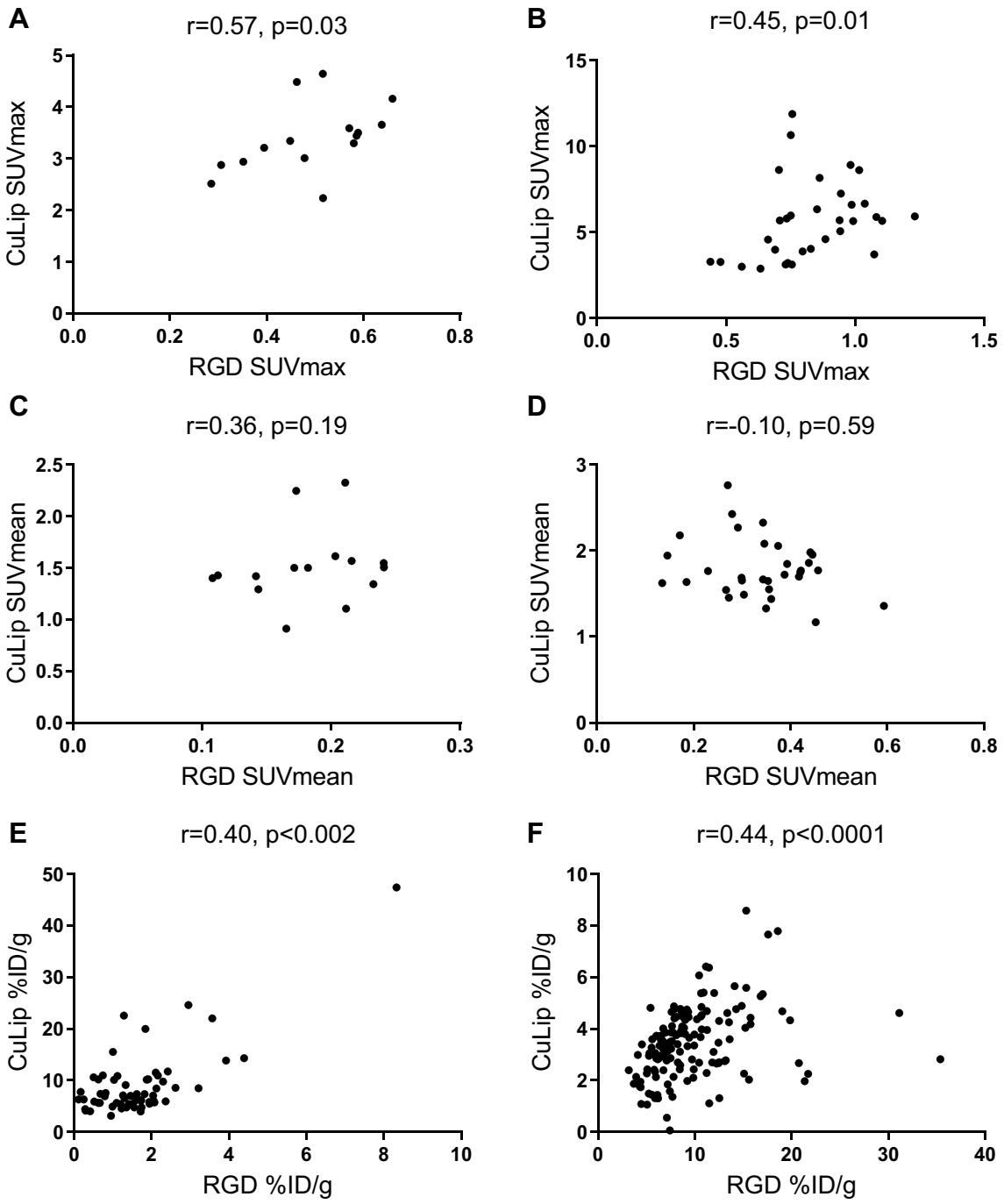

Figure 4 Spearman correlations of 24h ^{64}Cu-liposome and ^{68}Ga-RGD uptake in COLO 205 and CT26 tumors. COLO 205 PET ^{64}Cu-liposome vs RGD SUV_{max} (**A**), CT26 PET ^{64}Cu-liposome vs RGD SUV_{max} (**B**), COLO 205 PET ^{64}Cu-liposome vs RGD SUV_{mean} (**C**), CT26 PET ^{64}Cu-liposome vs RGD SUV_{mean} (**D**), COLO 205 gamma counted ^{64}Cu-liposome vs RGD %ID/g (**E**) and CT26 gamma counted ^{64}Cu-liposome vs RGD %ID/g (**F**).

IFP may decrease steeply from the tumor center to the periphery,[41,42] and since ^{64}Cu-liposome uptake was based on the whole tumor volume in this study, the single central IFP measurement may not have been representative.

The tumor tissue structure associated with high diffusivity, such as a loose extracellular matrix, should also be associated with a high propensity for liposomes to accumulate. Therefore, it was similarly unexpected that the tumor ^{64}Cu-liposome accumulation did not correlate positively with the level of tumor diffusivity (Table 1). It has previously been shown that, after accumulating in the tumor due to high vascular permeability, liposomes will stay in the near perivascular area[43] and our results indicate that liposomes will accumulate in tumors independent of tumor diffusivity. Importantly,

however, both tumor types in the current study showed relatively low levels of diffusivity (Figure 1). A study by Hompland et al found that IFP correlates with diffusivity only in A-07 melanoma xenografts, which showed high diffusivity.[44] They could not demonstrate a correlation in R-18 xenografts, which showed very low diffusivity, similar to the levels in the current study. Thus, the observed lack of correlation between diffusivity and ^{64}Cu-liposome accumulation in the current study may be due to the general low diffusivity in both tumor types. Also, diffusivity was evaluated in only a central tumor slice, whereas PET uptake was based on the whole tumor volume. We are not aware of any previous publications directly comparing dw-MRI and tumor liposome accumulation.

FDG uptake was higher in CT26 tumors than COLO 205 tumors (Figure 1), which was expected, as fast growing CT26 tumors are likely to have a high metabolic activity.[45] However, FDG and ^{64}Cu-liposome uptake did not correlate for neither CT26 nor COLO 205 tumors (Table 1), suggesting that tumor metabolic activity and the EPR-effect are not directly associated. No previous publications have correlated FDG uptake and liposome accumulation, but two publications with a different research focus have co-imaged experimental tumors with ^{64}Cu-liposome and ^{18}F-FDG PET/CT.[46,47]

A study limitation is the sequential imaging instead of simultaneous imaging, which meant that tumor growth between imaging sessions could potentially have influenced our results. The nature of PET radiotracers unfortunately precludes new imaging sessions prior to adequate decay of the previous radioisotope, so simultaneous imaging could not have been undertaken practically.

Due to the tumor sizes and resolution of PET images, the PET uptake was not correlated at a voxel-to-voxel level, but instead compared using overall uptake. We compensated for this limitation by correlating gamma counted uptake of ^{64}Cu and ^{68}Ga in small tumor pieces to give micro-regional information. In future studies, it would be interesting to perform ^{68}Ga-RGD and ^{64}Cu-liposome PET/CT imaging in a tumor model large enough for precise coregistration of PET/CT images. This will allow for direct voxel-to-voxel correlations to provide more information on the co-localization of neoangiogenesis and liposome accumulation.

The experimental nature of the tumor types provides an additional challenge for the conclusions, as they have neither the heterogeneous nature nor the compatible stromal component of spontaneous cancers.

Our results suggest that neoangiogenesis and liposome accumulation are, as expected, associated to some degree. This indicates that anticancer therapy-associated changes in angiogenesis could secondarily affect the EPR-effect, and that loss of effectiveness of liposomal chemotherapy may in some instances be explained by changes in tumor vasculature. This could be further investigated by performing combined ^{68}Ga-RGD and ^{64}Cu-liposome PET/CT imaging in combination with anti-angiogenic therapies, such as bevacizumab, metronomic cyclophosphamide or external beam radiotherapy.

Conclusion

Based on molecular imaging and gamma counting, a positive correlation between neoangiogenesis and the EPR-effect was identified for SUV_{max} and ID%/g, but not SUV_{mean}. We did not identify other microenvironmental factors that could help explain EPR variations, however, the strong theoretical basis for correlations with diffusivity and IFP means that these factors should probably not be ruled out at this point.

The correlation between ^{68}Ga-RGD and ^{64}Cu-liposome was only moderate, and ^{68}Ga-RGD probably cannot stand alone as a surrogate imaging marker for quantifying the EPR-effect and stratifying cancer patients before liposomal chemotherapy in a clinical setting.

In future studies, it would be interesting to repeat the current setup in a large spontaneous tumor model in order to substantiate the correlation between neoangiogenesis and the EPR-effect, as well as to perform studies combining the two tracers with anti-angiogenic therapy.

Disclosure

Financial support was provided by the Danish Strategic Research Council (NABIIT) ref. 2106-07-0033, the Lundbeck Foundation and the European Council (ERC grant). Annemarie Thuri Kristensen reports grants from Danish Technical University, during the conduct of the study; grants from Novo Nordisk A/S, grants from Copenhagen ZOO, grants from Independent Research Fund Denmark, outside the submitted work. The authors report no other potential conflicts of interest in this work.

References

1. Matsumura Y, Maeda H. A new concept for macromolecular therapeutics in cancer chemotherapy: mechanism of tumoritropic accumulation of proteins and the antitumor agent smancs. *Cancer Res*. 1986;46(12 Pt 1):6387–6392. doi:10.1021/bc100070g
2. Nichols JW, Bae YH. EPR: evidence and fallacy. *J Control Release*. 2014;190:451–464. doi:10.1016/j.jconrel.2014.03.057
3. Harrington KJ, Mohammadtaghi S, Uster PS, et al. Effective targeting of solid tumors in patients with locally advanced cancers by radiolabeled pegylated liposomes. *Clin Cancer Res*. 2001;7(2):243–254.

4. Presant CA, Blayney D, Kennedy P, et al. Preliminary report: imaging of Kaposi sarcoma and lymphoma in AIDS with indium-111-labelled liposomes. *Lancet*. 1990;335(8701):1307–1309. doi:10.1016/0140-6736(90)91188-G
5. Khalifa A, Dodds D, Rampling R, Paterson J, Murray T. Liposomal distribution in malignant glioma: possibilities for therapy. *Nucl Med Commun*. 1997;18(1):17–23.
6. Briele B, Hotze A, Oehr P, et al. Tumour imaging with labelled liposomes. *Lancet*. 1990;336(8719):875–876.
7. Lee H, Shields AF, Siegel BA, et al. 64Cu-MM-302 Positron Emission Tomography Quantifies Variability of Enhanced Permeability and Retention of Nanoparticles in Relation to Treatment Response in Patients with Metastatic Breast Cancer. *Clin Cancer Res*. 2017;23(15):4190–4203. doi:10.1158/1078-0432.CCR-16-3193
8. Lee H, Gaddy D, Ventura M, et al. Companion Diagnostic 64Cu-Liposome Positron Emission Tomography Enables Characterization of Drug Delivery to Tumors and Predicts Response to Cancer Nanomedicines. *Theranostics*. 2018;8:9. doi:10.7150/thno.21670
9. Petersen AL, Binderup T, Rasmussen P, et al. 64Cu loaded liposomes as positron emission tomography imaging agents. *Biomaterials*. 2011;32(9):2334–2341. doi:10.1016/j.biomaterials.2010.11.059
10. Hansen AE, Petersen AL, Henriksen JR, et al. Positron Emission Tomography Based Elucidation of the Enhanced Permeability and Retention Effect in Dogs with Cancer Using Copper-64 Liposomes. *ACS Nano*. 2015;9(7):6985–6995. doi:10.1021/acsnano.5b01324
11. Hare JI, Lammers T, Ashford MB, Puri S, Storm G, Barry ST. Challenges and strategies in anti-cancer nanomedicine development: an industry perspective. *Adv Drug Deliv Rev*. 2017;108:25–38. doi:10.1016/j.addr.2016.04.025
12. Veronese FM, Pasut G. PEGylation, successful approach to drug delivery. *Drug Discov Today*. 2005;10(21):1451–1458. doi:10.1016/s1359-6446(05)03575-0
13. Yang Q, Lai SK. Anti-PEG immunity: emergence, characteristics, and unaddressed questions. *Wiley Interdiscip Rev Nanomed Nanobiotechnol*. 2015;7(5):(October):655–677. doi:10.1002/wnan.1339
14. Abu Lila AS, Kiwada H, Ishida T. The accelerated blood clearance (ABC) phenomenon: clinical challenge and approaches to manage. *J Control Release*. 2013;172(1):38–47. doi:10.1016/j.jconrel.2013.07.026
15. Ishida T, Atobe K, Wang X, Kiwada H. Accelerated blood clearance of PEGylated liposomes upon repeated injections: effect of doxorubicin-encapsulation and high-dose first injection. *J Control Release*. 2006;115(3):251–258. doi:10.1016/j.jconrel.2006.08.017
16. Yang Q, Ma Y, Zhao Y, et al. Accelerated drug release and clearance of PEGylated epirubicin liposomes following repeated injections: A new challenge for sequential low-dose chemotherapy. *Int J Nanomedicine*. 2013;8:1257–1268. doi:10.2147/IJN.S41701
17. Børresen B, Henriksen JR, Clergeaud G, et al. Theranostic Imaging May Vaccinate against the Therapeutic Benefit of Long Circulating PEGylated Liposomes and Change Cargo Pharmacokinetics. *ACS Nano*. 2018;12(11):11386–11398. doi:10.1021/acsnano.8b06266
18. Jain RK, Stylianopoulos T. Delivering nanomedicine to solid tumors. *Nat Rev Clin Oncol*. 2010;7(11):653–664. doi:10.1038/nrclinonc.2010.139
19. Li Y, Wang J, Wientjes MG, Au JL-S. Delivery of nanomedicines to extracellular and intracellular compartments of a solid tumor. *Adv Drug Deliv Rev*. 2012;64(1):29–39. doi:10.1016/j.addr.2011.04.006
20. Brooks PC, Clark RA, Cheresh DA, Requirement of vascular integrin alpha v beta 3 for angiogenesis. *Science*. 1994;264(5158):569–571. doi:10.1126/science.7512751
21. Eliceiri BP, Cheresh DA. Role of alpha v integrins during angiogenesis. *Cancer J*. 2000;6(Suppl 3):S245.
22. Liu S. Radiolabeled multimeric cyclic RGD peptides as integrin alphavbeta3 targeted radiotracers for tumor imaging. *Mol Pharm*. 2009;3(5):472–487. doi:10.1021/mp060049x
23. Cai H, Conti PS. RGD-based PET tracers for imaging receptor integrin α vβ3 expression. *J Label Compd Radiopharm*. 2013;56(November2012):264–279. doi:10.1002/jlcr.2999
24. Gaertner FC, Kessler H, Wester HJ, Schwaiger M, Beer AJ. Radiolabelled RGD peptides for imaging and therapy. *Eur J Nucl Med Mol Imaging*. 2012;39(S1):(SUPPL.1):126–138. doi:10.1007/s00259-011-2028-1
25. Oxboel J, Brandt-Larsen M, Schjoeth-Eskesen C, et al. Comparison of two new angiogenesis PET tracers 68Ga-NODAGA-E[c(RGDyK)]2 and (64)Cu-NODAGA-E[c(RGDyK)]2; in vivo imaging studies in human xenograft tumors. *Nucl Med Biol*. 2014;41(3):259–267. doi:10.1016/j.nucmedbio.2013.12.003
26. Ozerdem U, Hargens AR. A simple method for measuring interstitial fluid pressure in cancer tissues. *Microvasc Res*. 2005;70(1–2):116–-120. doi:10.1016/j.mvr.2005.07.003
27. Mannelli L, Nougaret S, Vargas HA, Do RKG. Advances in diffusion-weighted imaging. *Radiol Clin North Am*. 2015;53(3):569–581. doi:10.1016/j.rcl.2015.01.002
28. Gambhir SS. Molecular imaging of cancer with positron emission tomography. *Nat Rev Cancer*. 2002;2(9):683–693. doi:10.1038/nrc882
29. Borza CM, Pozzi A, Borza DB, et al. Integrin alpha3beta1, a novel receptor for alpha3(IV) noncollagenous domain and a trans-dominant inhibitor for integrin alphavbeta3. *J Biol Chem*. 2006;281(30):20932–20939. doi:10.1074/jbc.M601147200
30. Goodman SL, Grote HJ, Wilm C. Matched rabbit monoclonal antibodies against v-series integrins reveal a novel alphavbeta3-LIBS epitope, and permit routine staining of archival paraffin samples of human tumors. *Biol Open*. 2012;1(4):329–340. doi:10.1242/bio.2012364
31. Henriksen JR, Petersen AL, Hansen AE, et al. Remote Loading of 64Cu2+ into Liposomes without the Use of Ion Transport Enhancers. *ACS Appl Mater Interfaces*. 2015;7(41):22796–22806. doi:10.1021/acsami.5b04612
32. Stapleton S, Allen C, Pintilie M, Jaffray DA. Tumor perfusion imaging predicts the intra-tumoral accumulation of liposomes. *J Control Release*. 2013;172(1):351–357. doi:10.1016/j.jconrel.2013.08.296
33. Ekdawi SN, Stewart JMP, Dunne M, et al. Spatial and temporal mapping of heterogeneity in liposome uptake and microvascular distribution in an orthotopic tumor xenograft model. *J Control Release*. 2015;207:101–111. doi:10.1016/j.jconrel.2015.04.006
34. Koukourakis MI, Koukouraki S, Giatromanolaki A, et al. Liposomal doxorubicin and conventionally fractionated radiotherapy in the treatment of locally advanced non-small-cell lung cancer and head and neck cancer. *J Clin Oncol*. 1999;17(11):3512–3521. doi:10.1200/JCO.1999.17.11.3512
35. Ogawara K, Un K, Minato K, Tanaka K-I, Higaki K, Kimura T. Determinants for in vivo anti-tumor effects of PEG liposomal doxorubicin: importance of vascular permeability within tumors. *Int J Pharm*. 2008;359(1–2):234–240. doi:10.1016/j.ijpharm.2008.03.025
36. Abu Lila AS, Matsumoto H, Doi Y, Nakamura H, Ishida T, Kiwada H. Tumor-type-dependent vascular permeability constitutes a potential impediment to the therapeutic efficacy of liposomal oxaliplatin. *Eur J Pharm Biopharm*. 2012;81(3):524–531. doi:10.1016/j.ejpb.2012.04.010
37. Karathanasis E, Chan L, Karumbaiah L, et al. Tumor vascular permeability to a nanoprobe correlates to tumor-specific expression levels of angiogenic markers. *PLoS One*. 2009;4(6):6. doi:10.1371/journal.pone.0005843
38. Yuan F, Dellian M, Fukumura D, et al. Vascular permeability in a human tumor xenograft: molecular size dependence and cutoff size. *Cancer Res*. 1995;55(17):3752–3756.
39. Heldin C-H, Rubin K, Pietras K, Ostman A. High interstitial fluid pressure - an obstacle in cancer therapy. *Nat Rev Cancer*. 2004;4(10):806–813. doi:10.1038/nrc1456

40. Gulliksrud K, Brurberg KG, Rofstad EK. Dynamic contrast-enhanced magnetic resonance imaging of tumor interstitial fluid pressure. *Radiother Oncol*. 2009;91(1):107–113. doi:10.1016/j.radonc.2008.08.015
41. Boucher Y, Baxter LT, Jain RK. Interstitial pressure gradients in tissue-isolated and subcutaneous tumors: implications for therapy. *Cancer Res*. 1990;50(15):4478–4484. doi:10.16373/j.cnki.ahr.150049
42. Jain RK. Transport of molecules in the tumor interstitium: a review. *Cancer Res*. 1987;47(12):3039–3051.
43. Yuan F, Leunig M, Huang SK, Berk DA, Papahadjopoulos D, Jain RK. Microvascular permeability and interstitial penetration of sterically stabilized (stealth) liposomes in a human tumor xenograft. *Cancer Res*. 1994;54(13):3352–3356.
44. Hompland T, Ellingsen C, Galappathi K. Rofstad EK. DW-MRI in assessment of the hypoxic fraction, interstitial fluid pressure, and metastatic propensity of melanoma xenografts. *BMC Cancer*. 2014;14(1):92. doi:10.1186/1471-2407-14-92
45. Kubota K. From tumor biology to clinical Pet: a review of positron emission tomography (PET) in oncology. *Ann Nucl Med*. 2001;15 (6):471–486.
46. Wong AW, Ormsby E, Zhang H, et al. A comparison of image contrast with (64)Cu-labeled long circulating liposomes and (18) F-FDG in a murine model of mammary carcinoma. *Am J Nucl Med Mol Imaging*. 2013;3(1):32–43.
47. Mahakian LM, Farwell DG, Zhang H, et al. Comparison of PET imaging with 64Cu-liposomes and 18F-FDG in the 7,12-dimethylbenz[a]anthracene (DMBA)-induced hamster buccal pouch model of oral dysplasia and squamous cell carcinoma. *Mol Imaging Biol*. 2014;16(2):284–292. doi:10.1007/s11307-013-0676-1